

# We are IntechOpen, the world's leading publisher of Open Access books Built by scientists, for scientists

5,000

Open access books available

125,000

International authors and editors

140M

Downloads

Our authors are among the

154

Countries delivered to

TOP 1%

most cited scientists

12.2%

Contributors from top 500 universities



WEB OF SCIENCE™

Selection of our books indexed in the Book Citation Index  
in Web of Science™ Core Collection (BKCI)

Interested in publishing with us?  
Contact [book.department@intechopen.com](mailto:book.department@intechopen.com)

Numbers displayed above are based on latest data collected.  
For more information visit [www.intechopen.com](http://www.intechopen.com)



# Biological Bone Micro Grinding Temperature Field under Nanoparticle Jet Mist Cooling

*Min Yang, Changhe Li, Liang Luo, Lan Dong, Dongzhou Jia, Runze Li, Mingzheng Liu, Xin Cui, Yali Hou, Yanbin Zhang, Teng Gao, Xiaoming Wang and Yunze Long*

## Abstract

Clinical neurosurgeons used micro grinding to remove bone tissues, and drip irrigation-type normal saline (NS) is used with low cooling efficiency. Osteonecrosis and irreversible thermal neural injury caused by excessively high grinding temperature are bottleneck problems in neurosurgery and have severely restricted the application of micro grinding in surgical procedures. Therefore, a nanoparticle jet mist cooling (NJMC) bio-bone micro grinding process is put forward in this chapter. The nanofluid convective heat transfer mechanism in the micro grinding zone is investigated, and heat transfer enhancement mechanism of solid nanoparticles and heat distribution mechanism in the micro grinding zone are revealed. On this basis, a temperature field model of NJMC bio-bone micro grinding is established. An experimental platform of NJMC bio-bone micro grinding is constructed, and bone micro grinding force and temperatures at different measuring points on the bone surface are measured. The results indicated that the model error of temperature field is 6.7%, theoretical analysis basically accorded with experimental results, thus certifying the correctness of the dynamic temperature field in NJMC bio-bone micro grinding.

**Keywords:** grinding, nanoparticle jet, mist cooling, biological bone, thermal injury, temperature field

## 1. Introduction

As a precise material removal method, grinding has been extensively applied to bone tissue removal and surface treatment in surgical procedures by conforming to the combining trend of machine science and biomedical science. In the machining field, the method of using miniature grinding tools (diameter is generally below 1 mm) for machining of feature size of 1~500  $\mu\text{m}$  is called micro grinding [1]. As bone tissues processed in osteological surgery are viable tissues and diamond grinding tool has obviously higher specific energy in the grinding process than other cutting methods, human bone, nerves, and blood vessels can be easily influenced by high temperature, and when grinding temperature is higher than 50°C, bone tissues

will experience irreversible necrosis, and nervous tissues will start experiencing thermal injury at 43°C [2]. In the present neurosurgery, surgeons usually perform drip irrigation of normal saline (NS) in the grinding zone following the following principle: The heat is carried away through convective heat transfer so as to cool the operative region. However, the drip irrigation-type cooling efficiency is not ideal; thermal injury in the operation process leads to necrosis of surrounding tissues and nerves, so the operation fails. The irreversible thermal injury of bone tissues triggered by high temperature in micro grinding is a bottleneck problem in bone micro grinding operation. Moreover, a large quantity of cooling liquid needs to be dripped into the grinding zone under drip irrigation-type cooling, which can easily reduce the visibility of the operative region under an endoscope [3].

In the machining field, as flood cooling grinding harms worker's health and the environment, dry grinding can easily result in serious burn of the specimen, and microdroplet jet grinding has insufficient cooling performance [4–7]; researchers have put forward nanoparticle jet mist cooling (NJMC) technique according to the theory of heat transfer enhancement, which cannot only enhance the convective heat transfer in the grinding zone by taking full advantages of high specific surface of nanoparticles and heat capacity but, meanwhile, can improve the tribological properties of the grinding zone and can reduce heat generation by virtue of superior antifriction and anti-wear characteristics and high bearing capacity of nanoparticles [8–10]. On this basis, as it is the fact that clinical surgical bone grinding has disadvantages of thermal injury and low visibility of operative region and that nanofluid microdroplet grinding has good cooling and lubrication effect with a small use level of cutting fluid in the machining field, the research team where the author joined proposed NJMC bio-bone micro grinding process: adding medical solid nanoparticles of a certain proportion into the NS and selecting the corresponding surface dispersant according to physical and chemical properties of nanoparticle material, supplemented by ultrasonic vibration, so medical nanoparticles can enjoy uniform and stable distribution in the NS so as to form a medical nanofluid under stable suspension, which is then sprayed into the focus grinding zone in jet form as carried by high-pressure gas via a miniature nozzle [11, 12]. And this is expected to lower the bone grinding temperature while improving the visibility of the operative region.

In recent years, researches have initially explored into thermal injury problem existing in the bio-bone grinding process. Taking heat transfer problem and its inverse problem in the bone grinding process with a miniature spherical grinding tool, Zhang et al. [13] conducted an in-depth study combining numerical simulation and experiment and analyzed the transient temperature field in the bone grinding process through a numerical simulation based on a heat generation model of bone grinding. Directing at the complex structure of bone issues and taking grinding temperature, grinding force, and blocking of grinding tool in the bone tissue grinding process as the study objects, Zhu et al. [14] obtained the grinding tool blocking mechanism in the bone tissue grinding by analyzing action rules of grinding temperatures on grinding temperature, grinding force, and grinding tool blocking. Sasaki et al. [15] analyzed heat generation during grinding using diamond tools with a diameter of 5 mm at a rotational speed of 100,000 r/min. They found that grinding for 10 cm along the grinding temperature without cooling liquid will expand the area of higher than 37.7°C continuously. To prevent thermal injuries to surrounding nerve tissues, Enomoto et al. [16] invented a new diamond spherical tool that can effectively reduce the temperature at the grinding zone. The surface of the diamond tool contains adsorbed super-hydrophilic TiO<sub>2</sub> nanoparticles, which effectively prevent temperature rise during bone grinding. The grinding zone is cooled during neurosurgery commonly by dripping a room-temperature NS into it.

The NS dissipates heat through natural heat convection, cooling the high-temperature region.

For the bottleneck problem in the current clinical neurosurgical bone operation, namely irreversible thermal injury, a NJMC bio-bone micro grinding process was put forward. The convective heat transfer mechanism of nanofluid in micro grinding zone was studied. A dynamic temperature field model in NJMC bio-bone grinding was constructed. By reference to the suppression measures of grinding thermal injury in the field of mechanical engineering, the bottleneck in orthopedic operation was solved so as to provide theoretical guidance and technical support for avoiding or reducing thermal injury in clinical orthopedic operation.

## 2. Grinding temperature field

Starting from the universal temperature field problem, the heat quantity  $Q$  at one spatial point takes place transiently, and the temperatures at other points nearby this point will be changed under the action of the transferred heat quantity, and meanwhile, they are variable due to the spatial-temporal change. Temperature field is a generic term of temperature distribution at spatial points at a certain time. Generally speaking, temperature field is a function of space and time [17]:

$$T = f(x, y, z, t) \quad (1)$$

Equation (1) denotes a three-dimensional (3D) unsteady-state temperature field where the object temperature is changed both in direction  $x$ ,  $y$ , and  $z$  and at time  $t$ . In this study, temperature field is divided into two types:

1. It is divided into steady-state temperature field and transient-state temperature field according to whether temperature changes with time. As indicated by Eq. (1), if the temperature field does not change with time, namely  $\frac{\partial T}{\partial t} = 0$ , it is a steady-state temperature field, or otherwise it is a transient-state temperature field. As mobile heat source is loaded, the temperature at specific point on the bone surface presents time-dependent change. Hence, the temperature field studied in this chapter is transient-state temperature field.
2. It is divided into temperature field in cut-in zone, that in steady-state zone and that in cut-out zone according to the grinding tool/specimen contact arc length. As shown in **Figure 1**, the effective cutting part of the grinding tool is totally within the length of the specimen material, the grinding tool/specimen contact arc length is  $l_c$ , and the temperature field is temperature field in steady-state zone. As the grinding process starts, the grinding tool/specimen

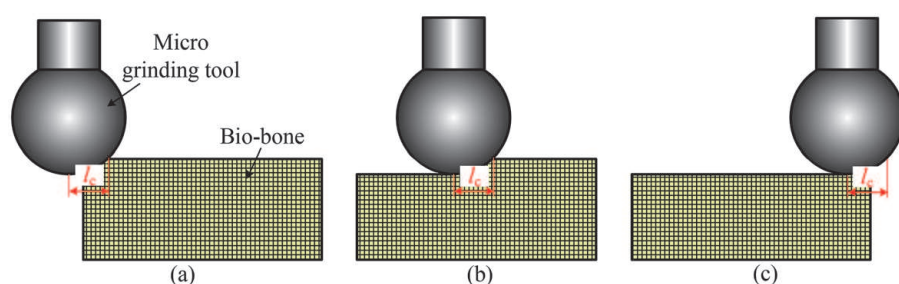


**Figure 1.** Schematic diagram of abrasive/bone contact states. (a) Cut-in zone. (b) Steady-state zone. (c) Cut-out zone.

contact arc length is gradually enlarged, but not reaching  $l_c$ , and at the moment, the grinding tool/specimen material is in cut-in phase, so the temperature field is in cut-in zone. As the grinding tool starts moving out of the specimen length, the contact arc length is gradually reduced to 0, and at the time, the grinding tool cuts out the specimen material, so the temperature is in cut-out zone.

## **2.1 The solution method of grinding temperature field**

The solving method of grinding temperature field includes analytical method and finite difference method.

### *2.1.1 Solution of grinding temperature field by analytical method*

Following the heat transfer theory and energy conservation law, analytical method solves the temperature rise function based on all kinds of boundary conditions in actual grinding machining so as to obtain temperature values on specimen surface and each internal node. The advantage of the analytical method is that it cannot only obtain the functional relationship regarding temperature distribution but also analyze different influence factors related to temperature field and their influence laws on temperature field distribution. Based on the theory of mobile heat source proposed by Jaeger [18] in 1942, many researchers have established theoretical grinding heat models with the main idea being superposition method of heat source temperature field. In other words, grinding interface is regarded as surface heat source constituted by numerous linear heat sources while linear heat sources are treated as a combination of numerous tiny unit linear heat sources, and each tiny unit linear heat source is simplified into combined action of point heat sources. Therefore, the basis for superposition method of heat source temperature fields is the solution of this temperature field at any time after transient point heat sources in an infinite object instantaneously emit partial heat quantity.

### *2.1.2 Solution of grinding temperature field by finite difference method*

As for solving the grinding temperature field, it can be complicated to use analytical method to solve even simple heat conduction problem. Grinding machining is itself of high complexity relative to other machining modes [19, 20], where input parameters of grinding temperature field are miscellaneous, abrasive particle distribution is irregular, grinding state of abrasive particle (plowing, sliding, cutting) is uncertain, cooling medium participates in convective heat transfer in the grinding zone, and surrounding airflow field of grinding tool has an effect on temperature. A large quantity of nonlinear coupling relations exists in the grinding process, so if any input parameter is changed, it will influence the follow-up derivation of expressions, and the solving of temperature field becomes even harder for the analytical method [21, 22]. Under this circumstance, the finite element method based on numerical method is a very effective method of solving heat conduction problem. It is only necessary to determine boundary conditions and initial conditions in order to conveniently calculate grinding temperature field, so it has been widely used by researchers at present. As the finite element method makes many hypotheses for grinding temperature field and boundary conditions, only specific built-in modules of specific software can be used [23], and the deviation of calculated grinding temperature from actual temperature is large. The finite element method based on numerical method is another effective method of calculating grinding temperature field between analytical method and finite element method.

It can accurately calculate temperature field through a theoretical modeling of boundary conditions of temperature field (heat flux, heat distribution ratio, convective heat transfer coefficient, etc.) according to actual grinding conditions. There have been few reports on calculation of grinding temperature field via finite difference method, so this method will be hereby described in details.

### 2.1.2.1 Basic principle of finite difference method

The object is divided into finite grid cells. A difference equation is obtained by transforming the differential equation, and the temperature at each grid cell node is solved through numerical simulation. As shown in **Figure 2**, under the 2D heat conduction problem, the object is divided into rectangular grids along directions  $x$  and  $y$  according to the spacing between  $\Delta x$  and  $\Delta y$ . The node is defined as intersection point of each grid line,  $p(i, j)$  denotes the position of each node,  $i$  is serial number at node along the direction  $x$ ,  $j$  is serial number at node along the direction  $y$ , and the intersection point between object boundary and grid is defined as boundary node. The basic principle of this method is to replace differential quotient with finite difference quotient so as to transform the original differential equation into a difference Equation [24].

### 2.1.2.2 Establishment of differential equation of heat conduction

In the grinding heat conduction problem, Fourier's law is the most fundamental heat conduction equation, namely the heat quantity passing through infinitesimal isothermal surface  $A$  within limited time interval  $t$  is  $Q$ , which is in direct proportion of temperature gradient  $\frac{\partial T}{\partial n}$  and is contrary to the direction of temperature field:

$$dQ = -k_w \frac{\partial T}{\partial n} dA dt \quad (2)$$

For heat flux:

$$q_x = -k_w \frac{\partial T}{\partial x} \quad (3)$$

where  $q_x$  is heat flux in direction  $x$  and  $\frac{\partial T}{\partial x}$  is temperature field in direction  $x$ .

The differential equation of heat conduction can be obtained according to Fourier's law and energy conservation law, and it is hypothesized that there is internal heat source in the object. Based on the above hypothesis, microelement

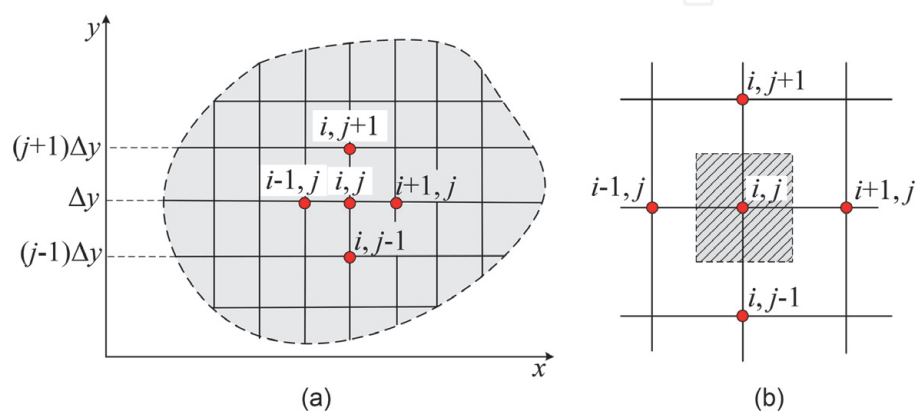


**Figure 2.** Schematic diagram of gridlines and nodes of finite difference method. (a) Grid element. (b) Grid node.

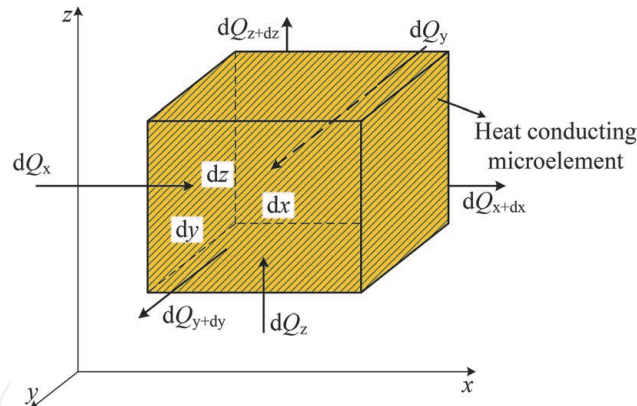


**Figure 3.**  
Schematic diagram of thermal conductive microelement.

$dV = dx$  is divided from the object under heat conduction. As shown in **Figure 3**, the three edges of this microelement are parallel to axes  $x$ ,  $y$ , and  $z$ , respectively. Thermal equilibrium analysis of the microelement is conducted. It can be known from the energy conservation law that the net heat quantity transferred in and out of the microelement within time  $dt$  should be equal to increment of internal energy in the microelement, namely net heat quantity transferred in and out of the microelement (I) and increment of internal energy in the microelement (II).

Net heat quantity transferred in and out of the microelement and increment of internal energy in the microelement will be, respectively, calculated as follows.

Energy equilibrium analysis is implemented for the microelement in **Figure 3**. The net quantity transferred in and out of the microelement can be obtained by adding the net heat quantities transferred in and out of the microelement from directions  $x$ ,  $y$ , and  $z$ , respectively. Along the direction of axis  $x$ , the heat quantity transferred in the microelement within time  $dt$  through plane  $x$  is:

$$dQ_x = q_x dydzdt \quad (4)$$

The heat quantity transferred out through plane  $x + dx$ :

$$dQ_{x+dx} = q_{x+dx} dydzdt \quad (5)$$

where  $q_{x+dx} = q_x + \frac{\partial q_x}{\partial x} dx$ .

Hence, the net heat quantity transferred in and out of the microelement along the direction of axis  $x$  within time  $dt$  is:

$$dQ_x - dQ_{x+dx} = -\frac{\partial q_x}{\partial x} dx dy dz dt \quad (6)$$

Similarly, the net quantities transferred in and out of the microelement along the directions of axes  $y$  and  $z$  within this time are, respectively:

$$dQ_y - dQ_{y+dy} = -\frac{\partial q_y}{\partial y} dx dy dz dt \quad (7)$$

$$dQ_z - dQ_{z+dz} = -\frac{\partial q_z}{\partial z} dx dy dz dt \quad (8)$$

The following is obtained by adding net quantities transferred in and out of the microelement in directions  $x$ ,  $y$ , and  $z$ :

$$I = -\left(\frac{\partial q_x}{\partial x} + \frac{\partial q_y}{\partial y} + \frac{\partial q_z}{\partial z}\right) dx dy dz dt \quad (9)$$

Within time  $dt$ , the increment of internal energy in the microelement is:

$$II = \rho c \frac{\partial T}{\partial t} dx dy dz dt \quad (10)$$

where  $\rho$  is density of point heat source heat conducting medium and  $c$  is the specific heat.

The three-dimensional heat conduction model can be obtained by Eqs. (9) and (10):

$$\frac{\partial T}{\partial t} = \alpha_t \left( \frac{\partial^2 T}{\partial x^2} + \frac{\partial^2 T}{\partial y^2} + \frac{\partial^2 T}{\partial z^2} \right) \quad (11)$$

where  $\alpha_t$  is thermal diffusion coefficient of point heat source heat conducting medium.

### 2.1.2.3 Differential equation converted into difference equation

This specimen is assumed as a rectangular plane, and it is discretely decomposed into a planar grid structure. Isometric spatial step length  $\Delta x = \Delta z = \Delta l$  is taken; two groups of equally spaced parallel lines are drawn to subdivide the rectangular specimen and the equation of parallel line:

$$\begin{cases} x = x_i = i\Delta l, i = 0, 1, \dots, M, M\Delta l = l_w \\ z = z_j = j\Delta l, j = 0, 1, \dots, N, N\Delta l = b_w \end{cases} \quad (12)$$

where  $x_i$  and  $z_j$  are coordinate value of transverse line  $i$  in direction  $x$  and coordinate value of vertical line  $j$  in direction  $z$ , respectively, and both lines constitute the difference grid;  $l_w$  and  $b_w$  are specimen length and height, respectively; and  $M$  and  $N$  are natural numbers.

The grid area of difference calculation is obtained through subdivision as shown in **Figure 3**.

A set of difference equations is built based on second-order difference quotient, namely:

$$\begin{cases} \frac{\partial^2 T}{\partial x^2}(i, j) = \frac{T(i+1, j) + T(i-1, j) - 2T(i, j)}{\Delta l^2} + O(\Delta l^2) \\ \frac{\partial^2 T}{\partial z^2}(i, j) = \frac{T(i, j+1) + T(i, j-1) - 2T(i, j)}{\Delta l^2} + O(\Delta l^2) \\ \frac{\partial T}{\partial t}(i, j) = \frac{T_{t+\Delta t}(i, j) - T_t(i, j)}{\Delta t} + O(\Delta t) \end{cases} \quad (13)$$

The difference equation of each node in the grid can be obtained:

$$\begin{aligned} T_{t+\Delta t}(i, j) = & \frac{\Delta t \{ k_x \cdot [T(i, j+1) + T(i, j-1)] + k_z \cdot [T(i+1, j) + T(i-1, j)] \}}{\rho_w c_w \Delta l^2} \\ & + \left[ 1 - \frac{2\Delta t(k_x + k_z)}{\rho_w c_w \Delta l^2} \right] T_t(i, j) \end{aligned} \quad (14)$$



## 2.2 Boundary condition

Heat transfer means transferring heat quantity from a system to another system with three main forms: convection, heat conduction, and radiation [25, 26]. The grinding tool/specimen contact interface is cooled with grinding fluid in the grinding process, so the grinding fluid flowing at this interface will conduct heat transfer on the specimen surface, where the main heat transfer form is convective heat transfer. As the grinding fluid contacts the specimen surface, partial heat quantity on the specimen surface is brought away by cooling fluid via convective heat transfer, and the residual heat stays on the specimen matrix and is transferred inside it. Therefore, the cooling effect of the machining zone can be strengthened by cooling fluid or by enhancing its heat transfer performance [27]. The temperature of external medium and convective heat transfer coefficient on boundary are given as shown in **Figure 4**. The heat quantity at grinding interface is generated due to grinding action of grinding tool and brought away by external cooling medium. In the meantime, both cooling medium and adjacent node  $(i-1, 1)$  on the specimen surface contact this node  $(i, 1)$ , so the heat quantity at this node will be transferred to cooling medium in convective way and also to adjacent node, and in the end, a stable temperature is reached at grinding tool/specimen interface [28].

The thermal equilibrium analysis of heat conduction in temperature field is to solve differential equation. The complete description of heat conduction process includes monodromy conditions and differential equation of heat conduction, where the former includes time condition, physical condition, geometrical condition, and boundary condition [29]. The boundary condition specifies characteristics of heat transfer process on object boundary, namely reflecting conditions for interaction between heat transfer process and surroundings, so initial condition (temperature at  $t = 0$ ) and boundary conditions (set temperature in boundary region or input and output heat fluxes) must be set in the temperature field. Based on the heat transfer theory, thermodynamic boundary conditions are generally divided into the three following types [30].

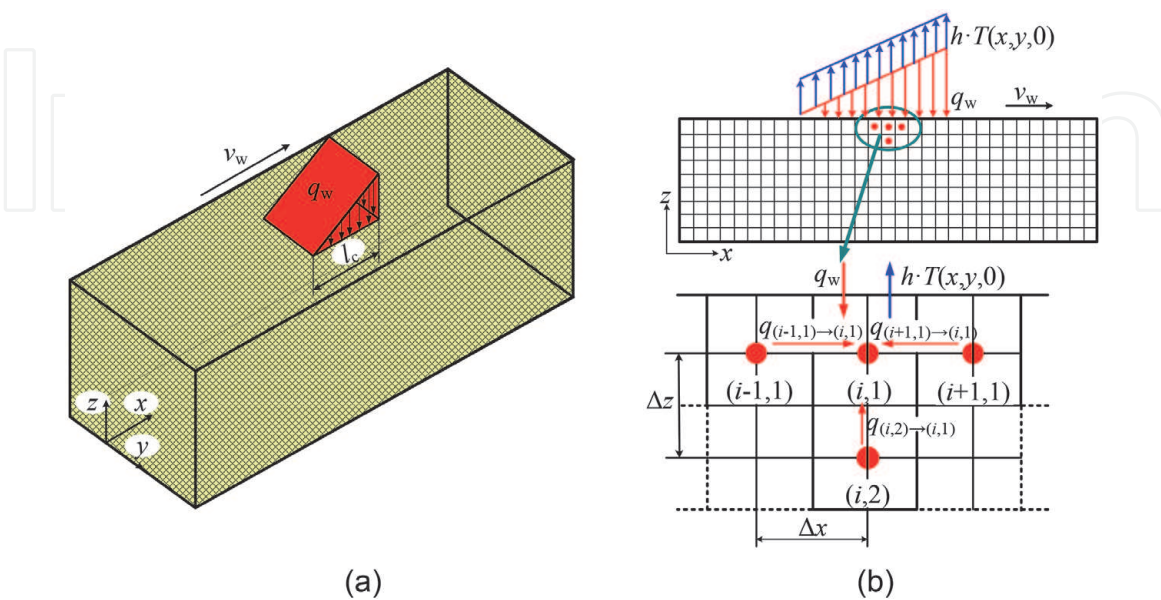


**Figure 4.** Schematic diagram of heat conduction model and convective heat transfer at grinding interface. (a) Heat conduction model. (b) Convective heat transfer at grinding interface.

### 2.2.1 The first kind of boundary conditions

Boundary condition of this type is forced convective boundary condition, namely temperature value at boundary of the given object at any time, and it is also called Dirichlet condition:

$$T|_{s_f} = T_w \quad (15)$$

where  $T_w$  is set temperature at boundary surface  $s_f$ . If boundary temperature is kept unchanged,  $T_w$  is a fixed value. If boundary temperature changes with time,  $T$  is a time-related functional expression.

### 2.2.2 The second kind of boundary conditions

Boundary condition of this type refers to heat flux on object boundary surface in normal direction at any time, and it is also called Neumann condition. The relationship between temperature gradient and heat flux is obtained through Fourier's law, and this is equivalent to temperature change rate on boundary  $s_f$  in normal direction at any time:

$$\left. \frac{\partial T}{\partial n} \right|_{s_f} = \frac{Q_w}{k} \quad (16)$$

where  $Q_w$  is heat quantity passing through boundary surface  $s_f$ .  $Q_w = 0$  when the boundary is under thermal insulation.  $Q_w$  is a fixed value when heat conduction at the boundary is constant, and it is a time-related function when the heat conduction changes with time.

Differential equation at the second type of boundary:

$$\frac{\partial}{\partial x} \left( k_x \cdot \frac{\partial T}{\partial x} \right) + \frac{\partial}{\partial y} \left( k_y \cdot \frac{\partial T}{\partial y} \right) + \frac{\partial}{\partial z} \left( k_z \cdot \frac{\partial T}{\partial z} \right) = Q_w \quad (17)$$

### 2.2.3 The third kind of boundary conditions

Boundary condition of this type denotes convective heat transfer between boundary surface and surrounding medium, and it is also called Robin condition. It can be known from Newton's law of cooling that convective heat transfer occurs between boundary layer of the specimen and cooling heat transfer medium:

$$h(T|_{z=0} - T_0) - k \left. \frac{\partial T}{\partial z} \right|_{z=0} = q_w \quad (18)$$

where  $q_w$  is convective heat flux at the boundary surface  $s_f$  between cooling heat transfer medium and specimen and  $h$  is convective heat transfer coefficient at the boundary between cooling heat transfer medium and specimen.

Differential equation at the third type of boundary:

$$\frac{\partial}{\partial x} \left( k_x \cdot \frac{\partial T}{\partial x} \right) + \frac{\partial}{\partial y} \left( k_y \cdot \frac{\partial T}{\partial y} \right) + \frac{\partial}{\partial z} \left( k_z \cdot \frac{\partial T}{\partial z} \right) = h(T|_{s_f} - T_f) \quad (19)$$

### 2.3 Heat distribution coefficients

An important problem exists in the establishment process of temperature field model in the grinding zone. It is necessary to determine the proportion of grinding heat quantity transferred into the specimen, namely heat distribution coefficient  $R_w$ . Under non-dry grinding condition as shown in **Figure 4**, the total heat quantity generated in the grinding zone is [31]:

$$q_{\text{total}} = \frac{F_t v_s}{b_g l_c} = q_w + q_g + q_c + q_f \quad (20)$$

where  $b_g$  is width of grinding tool;  $q_w$  is heat quantity staying on the specimen surface;  $q_g$  is heat quantity transferred into abrasive particle of grinding tool;  $q_c$  is heat quantity carried away by grinding chips; and  $q_f$  is heat quantity transferred out by cooling medium.

The heat distribution coefficient model proposed by Rowe in consideration of convective heat transfer in the grinding zone is generally applied. As indicated by the model, under high-efficiency deep grinding, total energy in the grinding zone is transferred into grinding tool, grinding chips, grinding fluid, and theoretical mathematical model of specimen material, and furthermore, its feasibility has been proved by a large quantity of experimental results.

Heat flux transferred into specimen, grinding tool, grinding fluid, and grinding chips is correlated with parameters like maximum contact temperature  $T_{\text{max}}$ , boiling point  $T_b$  of grinding fluid, and melting point  $T_m$  of specimen ( $T_{\text{max}} \leq T_b$ ) as shown in the following formula [32]:

$$\begin{cases} q_w = h_w \cdot T_{\text{max}} \\ q_g = h_g \cdot T_{\text{max}} \\ q_f = h_f \cdot T_{\text{max}} \\ q_c = h_d \cdot T_m \end{cases} \quad (21)$$

where  $h_w$ ,  $h_g$ ,  $h_f$ , and  $h_d$  are heat transfer coefficients of specimen material, grinding tool, grinding fluid, and grinding chips, respectively.

The proportion of heat quantity flowing into the specimen can be obtained as follows:

$$R_w = h_w \cdot T_{\text{max}} / q_{\text{total}} \quad (22)$$

## 3. Experimental study on micro grinding of biological bone with nanoparticle jet mist cooling

### 3.1 Nanoparticle jet mist cooling bone micro grinding experimental platform

**Figure 5** shows the established experimental platform of NJMC bio-bone micro grinding, including feed system, fixed system, cooling system, and measuring system. Both axes  $x$  and  $y$  of the 3D displacement device are Shinano stepper motors, and axis  $z$  is Panasonic servo braking motor. A 120# diamond grinding tool is used, where the diameter of grinding head is 1 mm. The mist cooling supply device is mist

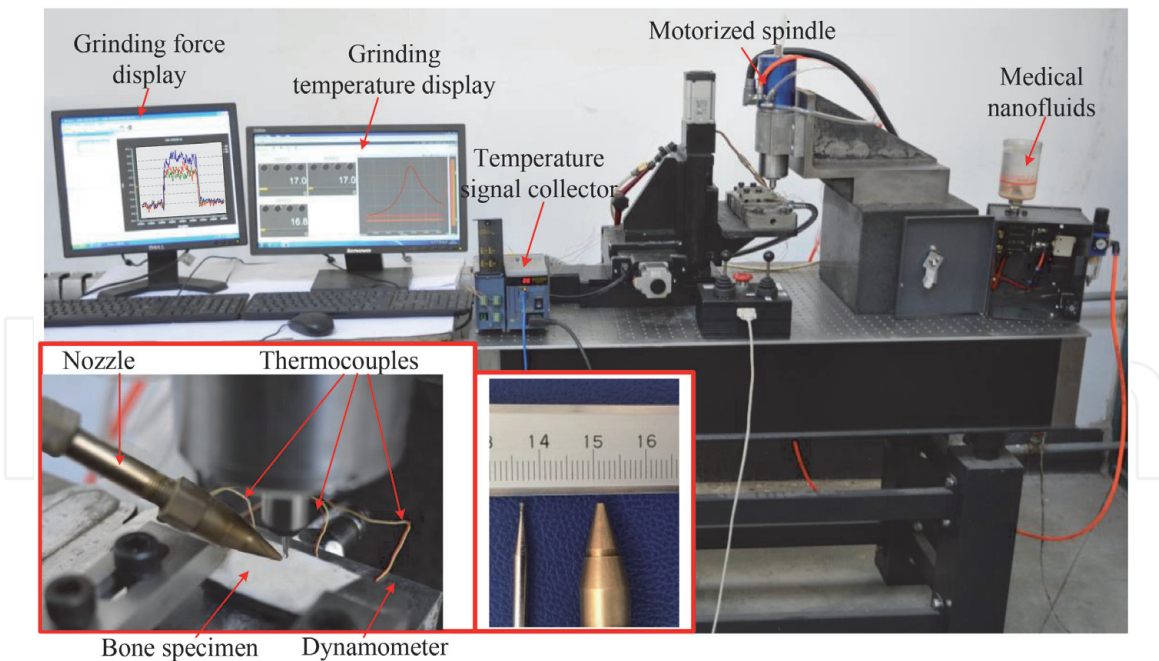


**Figure 5.**  
 Nanoparticle jet mist cooling bone micro grinding experimental platform.

cooling supply system produced by Shanghai KINS Energy-Saving Technology Co., Ltd. The jet parameters are uniformly set in the experiment as shown in **Table 1**.

The clamping mode of thermocouple: a blind hole drilled on the back face of the bone specimen has a certain distance from the bone surface (grinding depth), the thermocouple wire is placed into the blind hole, the bone specimen is fixed on the dynamometer, and the force and temperature in the micro bone grinding process are simultaneously measured. Thermocouple type is K (TT-K-30), and measuring frequencies of both dynamometer and thermocouple are 100 Hz.

In the biomedical field, HA, SiO<sub>2</sub>, and Al<sub>2</sub>O<sub>3</sub> nanoparticles feature nontoxicity and good biological compatibility and are commonly used drug carriers in nanodrug release system [33, 34]; NS is a common clinically used cooling medium as osmotic pressure is basically equal to osmotic pressure of human plasma. Therefore, HA, SiO<sub>2</sub>, and Al<sub>2</sub>O<sub>3</sub> nanoparticles with a diameter of 50 nm were used as solid nanoscale additives and NS as a nanofluid base to prepare HA, SiO<sub>2</sub>, and Al<sub>2</sub>O<sub>3</sub> nanofluids. Polyethylene glycol 400 has been extensively applied to lubrication in colonoscopy and gastroscopy by virtue of superior lubricating property and nontoxicity, and its safety in human body has been clinically certified. In the meantime, PEG400 also has good dispersity. Therefore, PEG400 was used as dispersing agent in this

Jet parameters	Value
Nozzle diameter	$d_0 = 1 \text{ mm}$
Compressed gas pressure	$\Delta p = 0.5 \text{ MPa}$
Feed flow rate	$Q_f = 50 \text{ mL/h}$
Spray inclination angle	$\beta = 15^\circ$
Nozzle height	$H = 0.6 \text{ mm}$
Spray cone angle	$\alpha = 27^\circ$

**Table 1.**  
 Table of mist cooling jet parameters.

chapter. When the dispersing agent with volume fraction of 2 vol.% and 2 vol.% is used, the suspension stability of the nanofluid will be the best. Hence, the nanofluid preparation method in this chapter was “two-step method,” namely adding 2 mL of HA, SiO<sub>2</sub>, and Al<sub>2</sub>O<sub>3</sub> nanoparticles and 0.2 mL of PE in 100 mL of NS supplemented with ultrasonic vibration for 15 min.

### 3.2 Temperature field of bio-bone micro grinding with different cooling methods

The dynamic temperature field model of NJMC bone grinding was verified. Different cooling modes were adopted: dry grinding, mist, and NJMC. As dynamic heat flux was loaded to theoretically calculate grinding temperature field, temperatures at different measuring points on the surface of the bone material were measured. As shown in **Figure 6**, three groups of thermocouples were used to simultaneously measure the temperatures at three measuring points—T1, T2, and T3—with spacing of 5 mm.

**Figure 7(a)** shows typical grinding force signals measured under dry grinding condition, where  $F_y$  is the force used to generate heat quantity.

The temperature field of bone micro grinding is solved under initial condition (room temperature) of  $T_0 = 20^\circ\text{C}$ . **Figure 8(a)** shows temperature curves measured at different measuring points under dry grinding condition and theoretical temperature curves. It can be known that in the bone grinding temperature curves, the peak values at three measuring points are  $36.1^\circ\text{C}$ ,  $38.2^\circ\text{C}$ , and  $36^\circ\text{C}$ , respectively, and measured peak values at the three measuring points are  $36.7^\circ\text{C}$ ,  $38.5^\circ\text{C}$ , and  $36.6^\circ\text{C}$ , respectively, namely the temperature on bone surface is ever-changing.

**Figure 8(b)** and **(c)** show peak values measured through the experiment at three measuring points under mist and NJMC conditions and those obtained through calculation. It can be known that in comparison with average temperature ( $36.8^\circ\text{C}$ ) on bone surface under dry grinding condition, the temperatures on the bone surface under mist and NJMC decline by 13.6% and 33.9%, respectively, thus proving the superior cooling effect of NJMC mode. The temperature error is 6.7%, and theoretical analysis basically accords with experimental result, which verifies the correctness of the dynamic temperature field in NJMC bio-bone micro grinding [35].

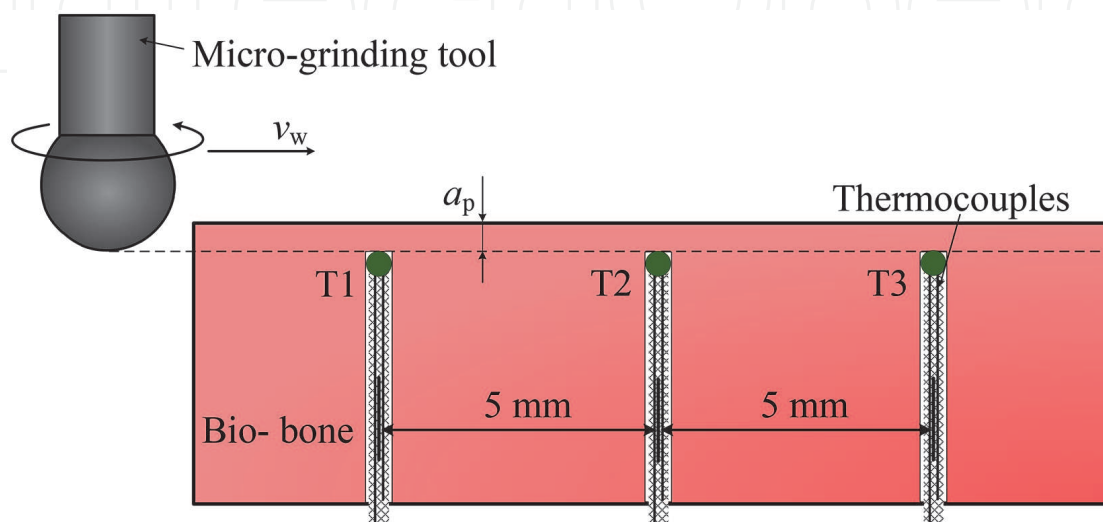


**Figure 6.** Schematic diagram of thermocouple clamping at different measuring points on bone surface.

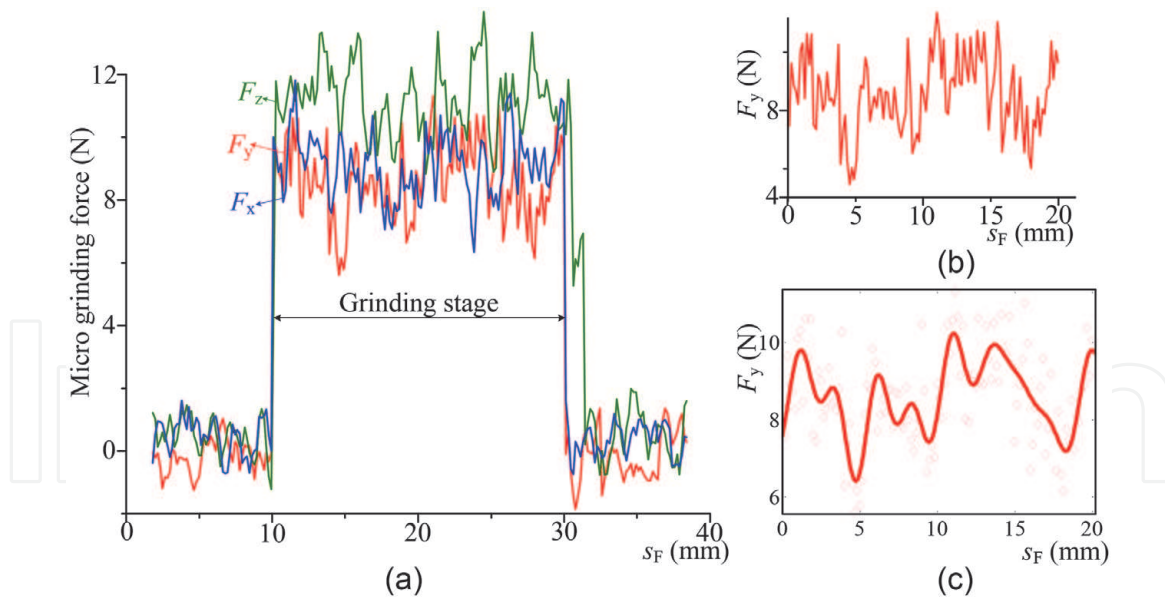


**Figure 7.** Typical force signals in micro grinding of biological bone materials. (a) Typical force signal of bio-bone micro grinding. (b) Grinding force in y direction. (c) Fitting curve of grinding force in y direction.

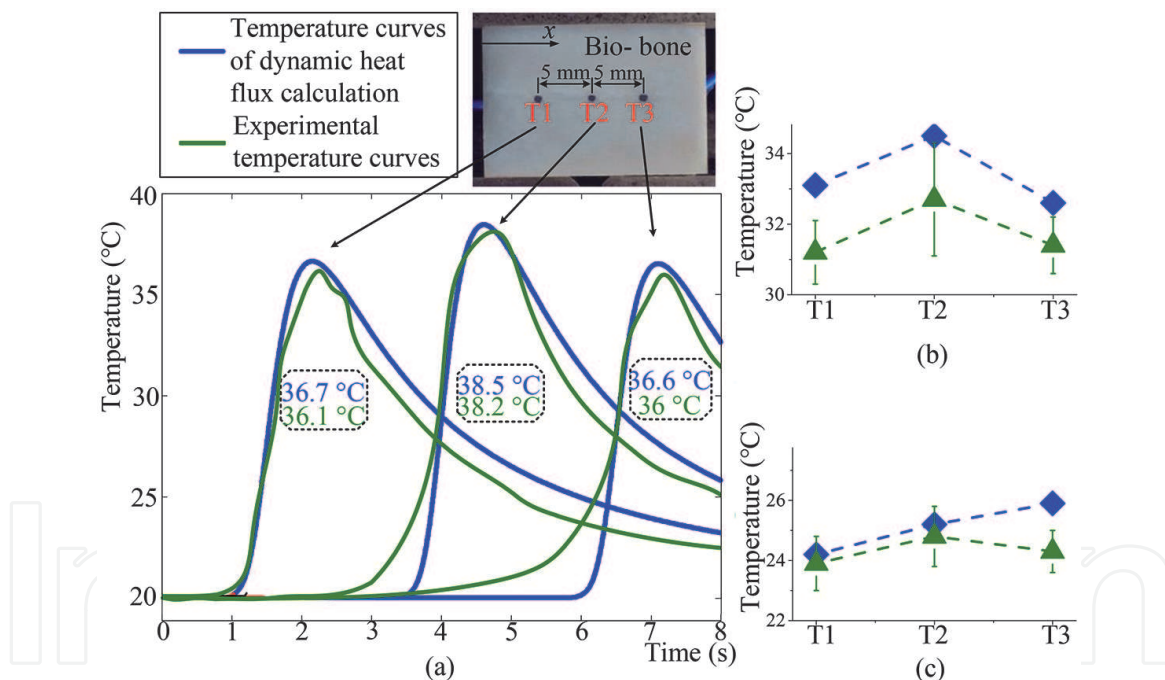


**Figure 8.** Temperature curves and values of different measuring points on bone surface under different cooling conditions. (a) Dry grinding temperature. (b) Mist cooling grinding temperature. (c) NJMC grinding temperature.

In order to explore into the dynamic characteristics of temperature field in bio-bone micro grinding, temperature fields in cut-in zone, steady-state zone, and cut-out zone are, respectively, analyzed. **Figures 9** and **10** show temperature fields and temperature curves in bone grinding under NJMC conditions. The detailed analysis process is as follows:

1. Cut-in zone: As shown in **Figures 9(a)** and **10**, as the grinding starts, the grinding tool starts contacting the material and gradually cuts into the material, undeformed cutting thickness is gradually increasing [36, 37], and the heat quantity generated at grinding interface starts migrating into the

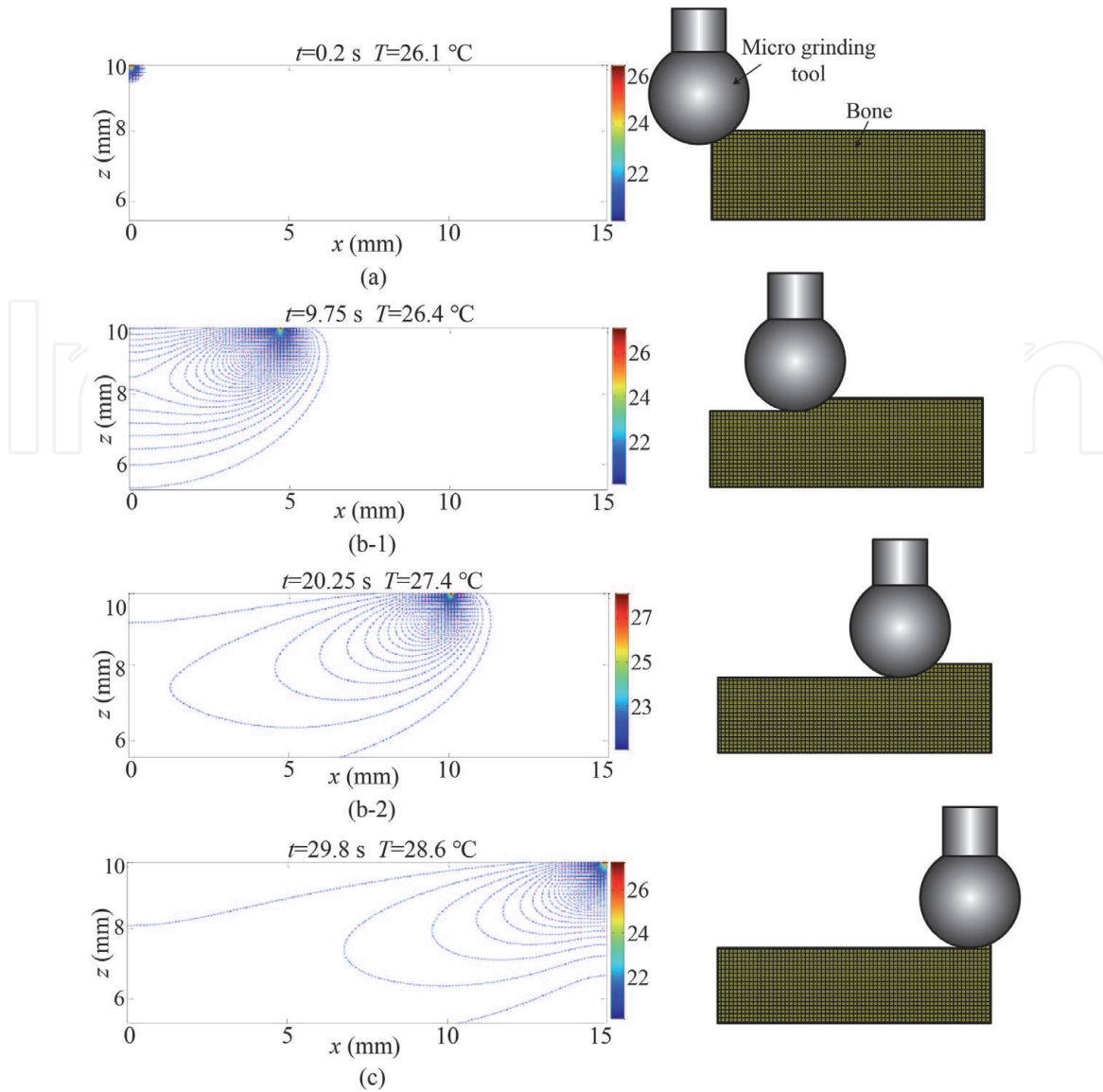


**Figure 9.** Temperature field in cut-in, steady-state, and cut-out zones of bone micro grinding. (a) Cut-in temperature field. (b-1) Steady-state temperature field. (b-2) Steady-state temperature field. (c) Cut-out temperature field.

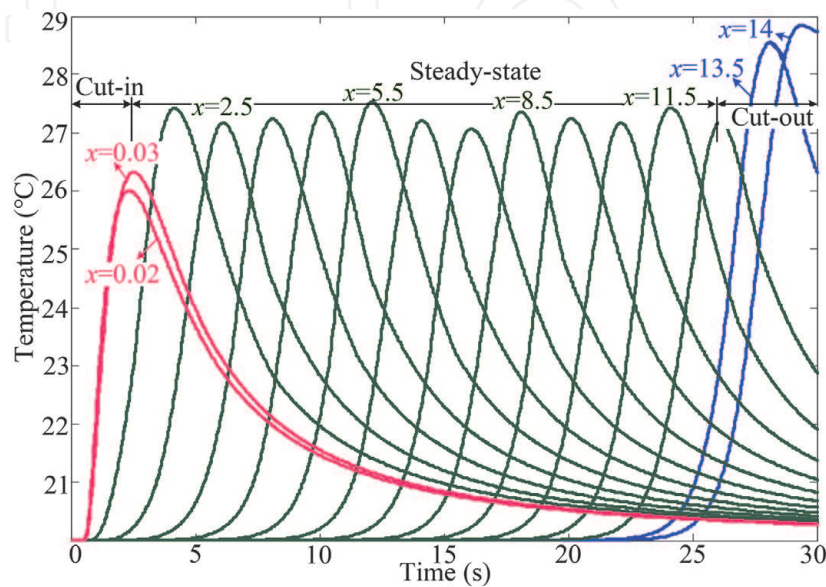


**Figure 10.** Temperature curves of cut-in, steady-state, and cut-out zones in bone micro grinding.

specimen surface. The temperature is low in the grinding zone, because the volume of material participating in the grinding in the cut-in zone is small with a small energy consumption.

2. Steady-state zone: In **Figures 9(b), (c)** and **10**, undeformed cutting thickness is kept at average value, and surface temperature no longer continues to rise, namely the formed temperature field reaches a steady state. As for grinding temperature fields calculated by researchers previously, after constant heat flux is loaded, the temperature value under which a steady state is reached will not be changed. However, in the temperature field of bone micro grinding with loaded dynamic heat flux as shown in the figure, the temperature value is ever-changing after the steady state is reached [38, 39].

3. Cut-out zone: As shown in **Figures 9(d)** and **10**, according to the heat transfer theory, undeformed thickness is gradually reduced when the grinding tool is in cut-out zone, and the volume of specimen material participating in the grinding action is continuously reduced. If the heat quantity generated at grinding interface remains unchanged, the volume of the material to which heat is migrated in the cut-out zone is continuously reduced. As heat conductivity coefficient of air is extremely low, more heat is aggregated in the grinding zone, and then grinding temperature rises to a great extent.

### 3.3 Effect of nanoparticle size on bone micro grinding temperature

To probe into the influence laws of nanoparticle size on bone micro grinding temperature,  $\text{Al}_2\text{O}_3$  nanoparticles with particle sizes of 30, 50, 70, and 90 nm and NS were used to prepare nanofluids for bone grinding experiment and measure grinding force and temperature at measuring point T2 on the bone surface.

**Figure 11(a)** shows theoretical temperature curves under different cooling conditions, where abscissa axis denotes dimensionless distance ( $x/l = 2v_w t/l_c$ ,  $2l = l_c$ ), namely the location of this point in the grinding arc zone [40, 41]. It can be known from the figure that at the entry end in the contact zone, grinding temperature abruptly increases, peak temperature deviates from central position of heat source on the curve and deflects toward exit end of the contact zone, and the temperature at the exit end in the contact zone declines slowly. **Figure 11(b)** shows bone grinding temperatures measured using nanoparticles with different particle sizes, and it can be known that the grinding temperature increases with nanoparticle size.

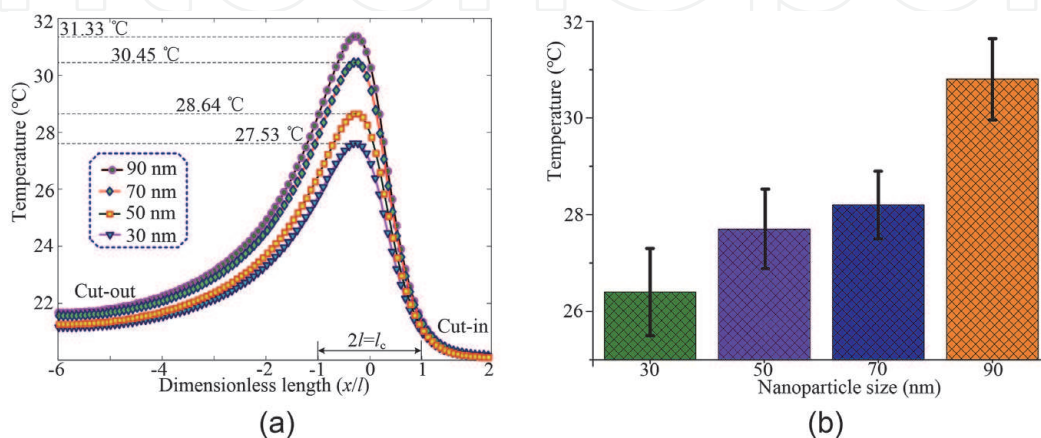


**Figure 11.** Micro grinding temperature with different nanoparticle size. (a) Theoretical calculated temperature value (b) theoretical calculated temperature value.



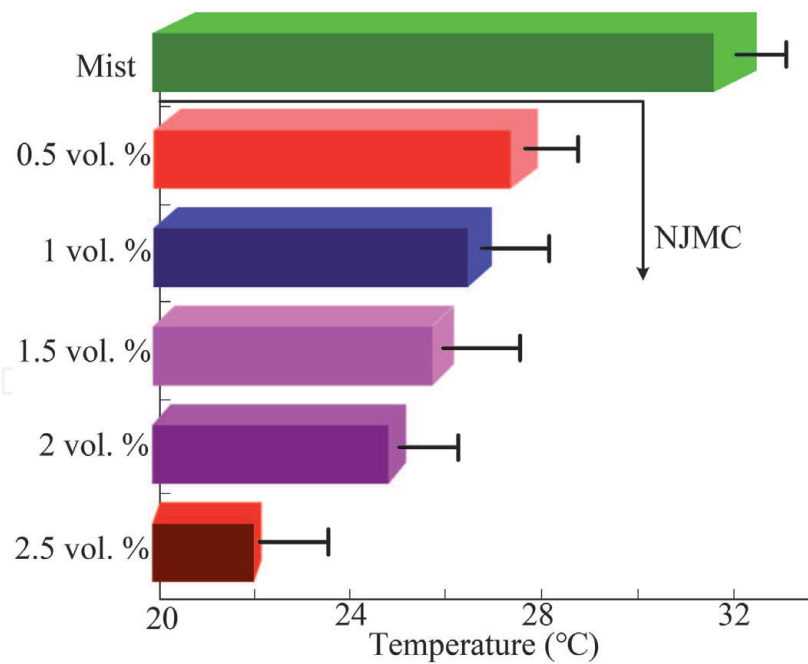


**Figure 12.**  
Temperature values measured with different concentration of nanoparticles.

### 3.4 Effect of nanoparticle concentration on bone micro grinding temperature

SiO<sub>2</sub> nanofluid with volume fraction of 0.5, 1, 1.5, 2, and 2.5 vol.% was prepared in the experiment to investigate the influence laws of nanoparticle concentration on bone micro grinding temperature. Mist cooling was taken for comparative experiment and to measure grinding force and temperature at measuring point T2.

As shown in **Figure 12**, the temperature measured under mist cooling is 32.7°C. Mist cooling is taken for control, and the surface temperature obtained using nanofluid with volume fraction of 0.5, 1, 1.5, 2, and 2.5 vol.% declines by 14.1%, 17.1%, 19.6%, 22.9%, and 33.3%, respectively, namely the surface temperature in micro grinding decreases as the nanoparticle volume fraction increases.

## 4. Conclusions

As irreversible thermal injury and poor visibility of operative region exist in the current clinical bone micro grinding operation, a NJMC bio-bone micro grinding process has been proposed to investigate the convective heat transfer mechanism of nanofluid in the grinding zone and reveal the heat distribution mechanism. On this basis, a dynamic temperature field model in NJMC bio-bone micro grinding process has been established. An experimental platform of NJMC bio-bone micro grinding process has been set up to realize an experimental verification of dynamic temperature fields in this grinding process, followed by an experimental study of influence of laws of nanoparticle size and concentration on bone grinding temperature. The following conclusions are drawn:

1. Heat distribution coefficient of specimen material, that of abrasive particle, that of grinding chips, and that of cooling medium, characterizes the abilities of heat transfer media to contend for heat quantity in the unit area of the grinding zone within unit time, so the heat distribution coefficient of the

specimen material can be expressed as the function of heat transfer coefficient of each heat transfer medium in the micro grinding zone.

2. Compared with average temperature (36.8°C) on bone surface under dry grinding condition, bone surface temperatures under mist cooling and NJMC conditions decrease by 13.6% and 33.9%, respectively, thus verifying the superior cooling effect of NJMC. The temperature error is 6.7%, theoretical analysis basically accords with experimental result, and thus the correctness of temperature field in NJMC bio-bone micro grinding is proved.
3. Al<sub>2</sub>O<sub>3</sub> nanoparticles with different particle sizes and NS were employed to prepare nanofluids for bone grinding experiment. According to the experimental results, the grinding temperature rose abruptly at entry end of the contact zone, the peak temperature value deviated from the central position of heat source on the curve and deflected toward the exit end of the contact zone, the temperature at the exit end of the contact zone declined slowly, and the grinding temperature increased with the nanoparticle size.
4. The bone grinding experiment has been carried out with nanofluids prepared using SiO<sub>2</sub> nanoparticles with different volume fractions and NS. In comparison with mist cooling, the surface temperatures obtained through nanofluids with nanoparticle volume fraction of 0.5, 1, 1.5, 2, and 2.5 vol.% declined by 14.1%, 17.1%, 19.6%, 22.9%, and 33.3%, respectively, namely the surface temperature declined as the nanoparticle volume fraction increased in grinding.

## Acknowledgements

This research was financially supported by the following organizations: the National Natural Science Foundation of China (51975305 and 51905289), the Major Research Project of Shandong Province (2019GSF108236, 2019GGX104040, and 2018GGX103044), the Shandong Provincial Natural Science Foundation of China (ZR2019PEE008), Major Science and Technology Innovation Engineering Projects of Shandong Province (2019JZZY020111), and Applied Basic Research Youth Project of Qingdao Science and Technology Plan (19-6-2-63-cg).

## Conflict of interests

The authors confirm that no conflict of interest exists in this chapter.

## Appendices and nomenclature

NJMC	nanoparticle jet mist cooling
$T_w$	set temperature at boundary surface
NS	normal saline
$Q_w$	heat quantity passing through boundary surface
3D	three-dimensional
$q_w$	convective heat flux at the boundary surface
$T$	grinding temperature
$h$	convective heat transfer coefficient at the boundary between cooling heat transfer medium and specimen

$x, y, z$	spatial coordinates
$b_g$	width of grinding tool
$t$	time
$q_w$	heat quantity staying on the specimen surface
$l_c$	contact arc length
$q_g$	heat quantity transferred into abrasive particle of grinding tool
$Q$	the heat quantity passing through infinitesimal isothermal surface
$q_c$	heat quantity carried away by grinding chips
$q_x$	heat flux in direction x
$q_f$	heat quantity transferred out by cooling medium
$\rho$	density of point heat source heat conducting medium
$T_{\max}$	maximum contact temperature
$c$	specific heat of point heat source heat conducting medium
$T_b$	boiling point of grinding fluid
$\alpha_t$	thermal diffusion coefficient of point heat source heat conducting medium
$T_m$	melting point of specimen
$l$	isometric spatial step length
$h_w$	heat transfer coefficients of specimen material
$l_w$	specimen length
$h_g$	heat transfer coefficients of grinding tool
$b_w$	specimen height
$h_f$	heat transfer coefficients of grinding fluid
$M, N$	natural numbers
$h_d$	heat transfer coefficients of grinding chips
$s_f$	convection heat transfer boundary surface
$R_w$	the proportion of heat quantity flowing into the specimen

IntechOpen

IntechOpen

## Author details

Min Yang<sup>1</sup>, Changhe Li<sup>1\*</sup>, Liang Luo<sup>2</sup>, Lan Dong<sup>3</sup>, Dongzhou Jia<sup>4</sup>, Runze Li<sup>5</sup>, Mingzheng Liu<sup>1</sup>, Xin Cui<sup>1</sup>, Yali Hou<sup>1</sup>, Yanbin Zhang<sup>1</sup>, Teng Gao<sup>1</sup>, Xiaoming Wang<sup>1</sup> and Yunze Long<sup>6\*</sup>

1 School of Mechanical and Automotive Engineering, Qingdao University of Technology, Qingdao, China

2 Ningbo Sanhan Alloy Material Co., Ltd, Ningbo, China

3 School of Mechanical and Electrical Engineering, Qingdao Binhai University, Qingdao, China


4 School of Mechanical Engineering, Inner Mongolia University for Nationalities, Tongliao, China

5 Department of Biomedical Engineering, University of Southern California, Los Angeles, United States

6 School of Physical Sciences, Qingdao University, Qingdao, China

\*Address all correspondence to: [sy\\_lichanghe@163.com](mailto:sy_lichanghe@163.com) and [yunze.long@163.com](mailto:yunze.long@163.com)

## IntechOpen

© 2020 The Author(s). Licensee IntechOpen. Distributed under the terms of the Creative Commons Attribution - NonCommercial 4.0 License (<https://creativecommons.org/licenses/by-nc/4.0/>), which permits use, distribution and reproduction for non-commercial purposes, provided the original is properly cited. 

## References

- [1] Lee PH, Lee SW, Lim SH, et al. A study on thermal characteristics of micro-scale grinding process using nanofluid minimum quantity lubrication (MQL). *International Journal of Precision Engineering and Manufacturing*. 2015;**16**(9):1899-1909. DOI: 10.1007/s12541-015-0247-2
- [2] Feldmann A, Ganser P, Nolte L, et al. Orthogonal cutting of cortical bone: Temperature elevation and fracture toughness. *International Journal of Machine Tools and Manufacture*. 2017; **118-119**:1-11. DOI: 10.1016/j.ijmachtools.2017.03.009
- [3] Zhang L, Tai BL, Wang AC, et al. Mist cooling in neurosurgical bone grinding. *CIRP Annals - Manufacturing Technology*. 2013;**62**(1):367-370. DOI: 10.1016/j.cirp.2013.03.125
- [4] Jia DZ, Li CH, Zhang YB, et al. Experimental evaluation of surface topographies of NMQL grinding ZrO<sub>2</sub> ceramics combining multiangle ultrasonic vibration. *The International Journal of Advanced Manufacturing Technology*. 2019;**100**(1-4):457-473. DOI: 10.1007/s00170-018-2718-y
- [5] Yang M, Li CH, Zhang YB, et al. Effect of friction coefficient on chip thickness models in ductile-regime grinding of zirconia ceramics. *The International Journal of Advanced Manufacturing Technology*. 2019; **102**(5):2617-2632. DOI: 10.1007/s00170-019-03367-0
- [6] Yang M, Li CH, Zhang YB, et al. Predictive model for minimum chip thickness and size effect in single diamond grain grinding of zirconia ceramics under different lubricating conditions. *Ceramics International*. 2019;**45**(12):14908-14920. DOI: 10.1016/j.ceramint.2019.04.226
- [7] Yang M, Li CH, Zhang YB, et al. Maximum undeformed equivalent chip thickness for ductile-brittle transition of zirconia ceramics under different lubrication conditions. *International Journal of Machine Tools and Manufacture*. 2017;**122**:55-65. DOI: 10.1016/j.ijmachtools.2017.06.003
- [8] Zhang YB, Li CH, Yang M, et al. Experimental evaluation of cooling performance by friction coefficient and specific friction energy in nanofluid minimum quantity lubrication grinding with different types of vegetable oil. *Journal of Cleaner Production*. 2016;**139**: 685-705. DOI: 10.1016/j.jclepro.2016.08.073
- [9] Wu WT, Li CH, Yang M, et al. Specific energy and g ratio of grinding cemented carbide under different cooling and lubrication conditions. *The International Journal of Advanced Manufacturing Technology*. 2019;**105** (1-4):67-82. DOI: 10.1007/s00170-019-04156-5
- [10] Jia DZ, Li CH, Zhang YB, et al. Experimental research on the influence of the jet parameters of minimum quantity lubrication on the lubricating property of Ni-based alloy grinding. *International Journal of Advanced Manufacturing Technology*. 2016;**82**: 617-630. DOI: 10.1007/s00170-015-7381-y
- [11] Zhang YB, Li CH, Ji HJ, et al. Analysis of grinding mechanics and improved predictive force model based on material-removal and plastic-stacking mechanisms. *International Journal of Machine Tools and Manufacture*. 2017;**122**: 81-97. DOI: 10.1016/j.ijmachtools.2017.06.002
- [12] Cui X, Li CH, Zhang YB, et al. Tribological properties under the grinding wheel and workpiece interface by using graphene nanofluid lubricant. *The International Journal of Advanced*

Manufacturing Technology. 2019;**104**  
(9–12):3943-3958

[13] Zhang LH, Tai BL, Wang GJ, et al. Thermal model to investigate the temperature in bone grinding for skull base neurosurgery. *Medical Engineering & Physics*. 2013;**35**(10):1391-1398. DOI: 10.1016/j.medengphy.2013.03.023

[14] Zhu Z, Hu ZW, Zhang ZB, et al. Study on grinding force of bovine cortical bone by different grinding wheels. *Diamond & Abrasives Engineering*. 2014;**34**(5):13-16

[15] Sasaki M, Morris S, Goto T, et al. Spray-irrigation system attached to high-speed drills for simultaneous prevention of local heating and preservation of a clear operative field in spinal surgery. *Neurologia Medico-Chirurgica*. 2010;**50**(10):900-904. DOI: 10.2176/nmc.50.900

[16] Enomoto T, Shigeta H, Sugihara T, et al. A new surgical grinding wheel for suppressing grinding heat generation in bone resection. *CIRP Annals - Manufacturing Technology*. 2014;**63**(1): 305-308. DOI: 10.1016/j.cirp.2014.03.026

[17] Zhang XM, Ren ZP, Mei FM. *Heat Transfer*. Beijing: China Construction Industry Press; 1995. pp. 75-96

[18] Jaeger JC. Moving sources of heat and the temperature of sliding contacts. *Proceedings of the Royal Society of New South Wales*. 1942;**76**:203-224

[19] Li HN, Xie KG, Wu B, et al. Generation of textured diamond abrasive tools by continuous-wave CO<sub>2</sub> laser: Laser parameter effects and optimisation. *Journal of Materials Processing Technology*. 2020;**275**: 116279. DOI: 10.1016/j.jmatprotec.2019.116279

[20] Li HN, Yang Y, Zhao YJ, et al. On the periodicity of fixed-abrasive planetary lapping based on a generic

model. *Journal of Manufacturing Processes*. 2019;**44**:271-287. DOI: 10.1016/j.jmapro.2019.05.036

[21] Yang M, Li CH, Zhang YB, et al. Experimental research on microscale grinding temperature under different nanoparticle jet minimum quantity cooling. *Materials and Manufacturing Processes*. 2016;**32**:589-597. DOI: 10.1080/10426914.2016.1176198

[22] Gao T, Zhang XP, Li CH, et al. Surface morphology evaluation of multi-angle 2D ultrasonic vibration integrated with nanofluid minimum quantity lubrication grinding. *Journal of Manufacturing Processes*. 2020;**51**:44-61. DOI: 10.1016/j.jmapro.2020.01.024

[23] Zhang DK, Li CH, Zhang YB, et al. Experimental research on the energy ratio coefficient and specific grinding energy in nanoparticle jet MQL grinding. *International Journal of Advanced Manufacturing Technology*. 2015;**78**:1275-1288. DOI: 10.1007/s00170-014-6722-6

[24] Shen B. *Minimum Quantity Lubrication Grinding Using Nanofluids*. Michigan: The University of Michigan; 2008

[25] Malkin S, Guo C. Thermal analysis of grinding. *CIRP Annals - Manufacturing Technology*. 2007;**56**(2):760-782

[26] Kuwahara F, Shirota M, Nakayama A. A numerical study of interfacial convective heat transfer coefficient in two-energy equation model for convection in porous media. *International Journal of Heat and Mass Transfer*. 2001;**44**(6):1153-1159. DOI: 10.1016/s0017-9310(00)00166-6

[27] Duursma G, Sefiane K, Kennedy A. Experimental studies of nanofluid droplets in spray cooling. *Heat Transfer Engineering*. 2009;**30**(13):1108-1120. DOI: 10.1080/01457630902922467

- [28] Zhang DK, Li CH, Jia DZ, et al. Specific grinding energy and surface roughness of nanoparticle jet minimum quantity lubrication in grinding. *Chinese Journal of Aeronautics*. 2015;**28**(2): 570-581. DOI: 10.1016/j.cja.2014.12.035
- [29] Li HN, Axinte D. On a stochastically grain-discretised model for 2D/3D temperature mapping prediction in grinding. *International Journal of Machine Tools and Manufacture*. 2017; **116**:60-76. DOI: 10.1016/j.ijmachtools.2017.01.004
- [30] Yang SM, Tao WS. *Heat Transfer*. Higher Education Press: Beijing; 1998. pp. 33-296p
- [31] Outwater JQ, Shaw MC. Surface temperature in grinding. *ASME*. 1952; **12**(1):73-78
- [32] Rowe WB, Black SCE, Mills B, et al. Analysis of grinding temperatures by energy partitioning. *Proceedings of the Institution of Mechanical Engineers, Part B: Journal of Engineering Manufacture*. 1996;**210**(6):579-588
- [33] Yang YH, Liu CH, Liang YH, et al. Hollow mesoporous hydroxyapatite nanoparticles (hmHANPs) with enhanced drug loading and pH-responsive release properties for intracellular drug delivery. *Journal of Materials Chemistry B*. 2013;**1**(19): 2447-2450. DOI: 10.1039/c3tb20365d
- [34] Deng H, Lei Z. Preparation and characterization of hollow  $\text{Fe}_3\text{O}_4/\text{SiO}_2@$  PEG-PLA nanoparticles for drug delivery. *Composites Part B: Engineering*. 2013;**54**:194-199. DOI: 10.1016/j.compositesb.2013.05.010
- [35] Yang M, Li CH, Zhang YB, et al. Theoretical analysis and experimental research on temperature field of microscale bone grinding under nanoparticle jet mist cooling. *Journal of Mechanical Engineering*. 2018;**54**(18): 194-203. DOI: 10.3901/JME.2018.18.194
- [36] Yang M, Li CH, Zhang YB, et al. Thermodynamic mechanism of Nanofluid minimum quantity lubrication cooling grinding and temperature field models. In: Mohsen Sheikholeslami Kandelousi, *Microfluidics and Nanofluidics*. London: IntechOpen; 2018. pp. 61-81
- [37] Zhang YB, Li CH, Jia DZ, et al. Experimental evaluation of the lubrication performance of  $\text{MoS}_2/\text{CNT}$  nanofluid for minimal quantity lubrication in Ni-based alloy grinding. *International Journal of Machine Tools and Manufacture*. 2015;**99**:19-33. DOI: 10.1016/j.ijmachtools.2015.09.003
- [38] Gao T, Li CH, Zhang YB, et al. Dispersing mechanism and tribological performance of vegetable oil-based CNT nanofluids with different surfactants. *Tribology International*. 2019;**131**:51-63. DOI: 10.1016/j.triboint.2018.10.025
- [39] Zhang YB, Li CH, Jia DZ, et al. Experimental evaluation of  $\text{MoS}_2$  nanoparticles in jet MQL grinding with different types of vegetable oil as base oil. *Journal of Cleaner Production*. 2015; **87**:930-940. DOI: 10.1016/j.jclepro.2014.10.027
- [40] Lee PH, Nam JS, Li C, et al. An experimental study on micro-grinding process with nanofluid minimum quantity lubrication (MQL). *International Journal of Precision Engineering and Manufacturing*. 2012; **13**:331-338. DOI: 10.1007/s12541-012-0042-2
- [41] Yang M, Li CH, Zhang YB, et al. Research on microscale skull grinding temperature field under different cooling conditions. *Applied Thermal Engineering*. 2017;**126**:525-537. DOI: 10.1016/j.applthermaleng.2017.07.183